Title

Reversible inhibition of efflux transporters by hydrogel microdevices

Authors

Levy, Elizabeth S

Samy, Karen E

Lamson, Nicholas G

et al.

Publication Date

2019-12-01

DOI

10.1016/j.ejpb.2019.10.007

Peer reviewed

HHS Public Access

Author manuscript

Eur J Pharm Biopharm. Author manuscript; available in PMC 2020 December 01.

Published in final edited form as:

Eur J Pharm Biopharm. 2019 December ; 145: 76–84. doi:10.1016/j.ejpb.2019.10.007.

Reversible Inhibition of Efflux Transporters by Hydrogel Microdevices

Elizabeth S. Levy[a], **Karen E. Samy**[a,b], **Nicholas G. Lamson**[c], **Kathryn A. Whitehead**[c,d], **Deanna L. Kroetz**[a,*], **Tejal A. Desai**[a,b,*]

[a]Department of Bioengineering and Therapeutic Sciences, University of California, San Francisco, CA, USA

[b]UC Berkeley – UCSF Graduate Program in Bioengineering, UCSF Mission Bay Campus, San Francisco, CA, USA

[c]Department of Chemical Engineering, Carnegie Mellon University, Pittsburgh, PA, USA

[d]Department of Biomedical Engineering, Carnegie Mellon University, Pittsburgh, PA, USA

Abstract

Oral drug delivery is a preferred administration route due to its low cost, high patient compliance and fewer adverse events compared to intravenous administration. However, many pharmaceuticals suffer from poor solubility and low oral bioavailability. One major factor that contributes to low bioavailability are efflux transporters which prevent drug absorption through intestinal epithelial cells. P-glycoprotein (P-gp) and Breast Cancer Resistance Protein (BCRP) are two important efflux transporters in the intestine functioning to prevent toxic materials from entering systemic circulation. However, due to its broad substrate specificity, P-gp limits the absorption of many therapeutics, including chemotherapeutics and antibacterial agents. Methods to inhibit P-gp with competitive inhibitors have not been clinically successful. Here, we show that micron scale devices (microdevices) made from a commonly used biomaterial, polyethylene glycol (PEG), inhibit P-gp through a biosimilar mucus in Caco-2 cells and that transporter function is restored when the microdevices are removed. Microdevices were shown to inhibit P-gp mediated transport of calcein AM, doxorubicin, and rhodamine 123 (R123) and BCRP mediated transport of BODIPY-FL-prazosin. When in contact with Caco-2 cells, microdevices decrease the cell surface amount of P-gp without affecting the passive transport. Moreover, there was an increase in mucosal to serosal transport of R123 with microdevices in an *ex-vivo* mouse model and increased absorption *in vivo*. This biomaterial-based approach to inhibit efflux transporters can be applied to a range of drug delivery systems and allows for a nonpharmacologic method to increase intestinal drug absorption while limiting toxic effects.

*Corresponding author.

Competing interests

The authors declare no competing interests.

Introduction

Oral drug dosing is the preferred route of delivery due to its convenience, safety, and low cost.[1–4] However, many drugs suffer from poor solubility and low oral bioavailability which can limit their therapeutic effectiveness. Factors that contribute to low bioavailability are the low pH of the stomach, intestinal metabolizing enzymes leading to drug degradation, and the hydrophobic mucosal layer and efflux transporters preventing intestinal drug absorption.[1,5] Efflux transporters of the multigene ATP binding cassette (ABC) transporter family such as P-glycoprotein (P-gp), breast cancer resistance protein (BCRP), and multidrug resistance-associated protein 2 (MRP2) are expressed on the apical membrane of intestinal epithelial cells.[6] These transporters efflux absorbed compounds from the intestinal cells back into the gastrointestinal (GI) lumen, thus preventing them from reaching the systemic circulation.[6] Efflux transporters function to protect the small intestine from harmful toxins and xenobiotics by limiting their absorption.[7,8] However, most efflux transporters have broad substrate specificity which translates into poor oral bioavailability for a significant number of therapeutics.[6,8–10]

Many strategies have been employed to inhibit the function of efflux transporters to increase drug absorption.[7,11,12] P-gp is the most widely studied efflux transporter since it limits the bioavailability of numerous substrates, including chemotherapeutics, immunosuppressants and antimicrobial agents.[7] The main approaches studied for P-gp inhibition include competitive inhibitors that directly block the site of drug binding and noncompetitive inhibitors that either block the hydrolysis of adenosine triphosphate (ATP) necessary for P-gp function or allosterically interact to reduce P-gp activity.[7,13–15] However, decades of research aimed at targeting P-gp through the use of chemical inhibitors provide limited evidence for clinical applicability.[16,17] The lack of success using P-gp inhibitors to improve bioavailability underlies the ongoing search for safer and more effective methods to address this critical limitation in oral absorption.[15]

Micro- and nanotechnology-based drug delivery systems have been used as effective tools to increase drug absorption and enhance bioavailability.[4,18] Previously, we have shown that nanostructured thin films increase drug permeation through the intestinal epithelium.[19] We have also shown that microdevices increase residence time in the intestine and increase permeation, thus increasing drug bioavailability.[20] Additionally, hydrogels are widely used in drug delivery because of their biocompatibility, ease of tunability, and their ability to increase bioavailability, thus allowing for improved absorption in target regions.[21–25] In particular, PEG hydrogels are commonly used for oral drug delivery as PEG is non-immunogenic and biocompatible.[26–28] PEG based nanoparticles have been investigated for their ability to modulate permeability *in vitro*.[23] Additionally, PEG in a non-crosslinked form was shown to limit P-gp activity with evidence indicating the changes are due to alterations in the microenvironment of P-gp.[29] Altering the molecular weight of the non-crosslinked PEG has been shown to alter the degree of P-gp inhibition; however, there is not a clear correlation between PEG molecular weight and P-gp inhibition.[30,31] Hydrogel and polymer based microparticles, however, have a decreased residence time in the intestine which is limited by peristaltic flow that dislodges the hydrogel material.[32]

The overall goal of this study is to investigate the effects of hydrogel microdevices to improve drug absorption through gastrointestinal epithelial cells. Since PEG-based hydrogels are commonly used in various controlled release systems, gaining a basic understanding of their effects on efflux transporters is essential for the development of improved oral delivery systems. Biocompatible PEG-based drug delivery microdevices were developed and optimized for adherence to the intestinal epithelial wall and reversible inhibition of efflux transport. The data presented below supports this approach for maximizing drug absorption, increasing oral bioavailability, and limiting toxicity of orally administered substrates of P-gp and BCRP.

Materials & Methods

Fabrication of Microdevices

Microdevices with a diameter of 200 μm and a thickness of 20 μm were fabricated as previously described.[33] Briefly, a solution consisting of 80% w/v 750 number average molecular weight (Mn) polyethylene glycol dimethacrylate (PEGDMA) (Sigma-Aldrich), 10% w/v IRCAGURE (2-Hydroxy-4′-(2-hydroxyethoxy)-2-methylpropiophenone) (Sigma-Aldrich) in dimethyl sulfoxide (DMSO), and 10% w/v deionized water was added to the surface of a piranha cleaned 3” silicon wafer (Addison Engineering Inc) at a thickness of 20 μm. The wafer is brought into contact with a photomask with 200 μm exposed features and irradiated with a 365 nm UV light source using a Karl Suss Mask Aligner for 1 minute to crosslink the PEGDMA. The solution viscosity is important for appropriate spreading on the wafer. The wafer is then removed and the polymer that is not crosslinked is washed away in water. The microdevices are then removed from the wafer into ethanol. Prior to studies, microdevices are washed with sterile 2% Bovine Serum Albumin (BSA) solution (Sigma-Aldrich).

Cell Culture

Human colon adenocarcinoma cell line (Caco-2) purchased from ATCC was maintained in 2D cell culture as previously described.[19] Caco-2 cells between passage 5 and 13 were used for all experiments. Mycoplasma test was performed on the cell line and found to be negative. Cell culture experiments are performed in two formats, on transwells and 96 well plates. Cells are seeded at $75*10^3$ cells/cm^2 and cultured for 21 days for transwell experiments. For experiments performed in a 96 well plate, cells are seeded at $27*10^3$ cells/cm^2 and cultured for 14 days. Cell growth conditions were optimized so that P-gp expression levels between the transwells and 96 well plates were similar (Supporting Information 1).

Immunohistochemistry

Caco-2 cells cultured on transwells for 21 days were fixed as described previously.[19] DAPI (1:500) and Alexa 488 Phalloidin (1:200) (Life Technologies 1726566) were used to stain the cells. After staining, transwells were cut out and mounted on a slide with slowfade gold antifade reagent with DAPI (Invitrogen). Cells were imaged with a Tokagawa CSU22 spinning disk confocal microscope.

Transwell Culture

Caco-2 cells were seeded at $75*10^3$ cells/cm^2 on high density polycarbonate Transwell inserts (24-well, 0.4 uM pore size) (Corning) as described previously.[19] Cells were cultured for 21 days before use in experiments.

Viability Studies

Caco-2 cells were seeded at a density of $27*10^3$ cells/cm^2 on a 96 well plate. After 14 days of culture the cells were washed, and a PrestoBlue assay was performed. Briefly, microdevices were added to the wells and incubated for 3 hours. The microdevices were removed and PrestoBlue cell viability Reagent (Invitrogen) added to the wells. After a 10-minute incubation at 37°C the absorbance was read at 570 nm. Wells without microdevices were used as controls.

Dead cells were measured by propidium iodine (PI) staining. Cells were grown in a transwell for 21 days, after which microdevices were added for 3 hours. The cells were lifted by cell dissociation buffer and stained with 2 mg/mL PI for 5 minutes. The cells were washed 3X and placed in 2% BSA solution to run on flow cytometry (BD FACS Calibur).

An ATP assay kit (Abcam) was used to determine total levels of cellular ATP in Caco-2 cells grown on a transwell model for 21 days. Cells were treated in the absence or presence of microdevices for 3 hours. After 3 hours, phenol red free Minimum Essential Medium (MEM) (Gibco) is removed and detergent is added to lyse cells and stabilize ATP. Substrate solution provided by the kit is added and luminescence is measured after 15 minutes.

Transport Studies

The calcein AM assay was performed in a 96 well plate. Caco-2 cells were grown on 96 well plates for 2 weeks. After the cells were washed with phenol red free MEM, 3 μM calcein AM in the presence and absence of microdevices or CSA, positive control inhibitor of P-gp, was added to the wells and incubated at 37°C. After 1 or 3 hours the cells were lysed to determine the intracellular calcein concentration. Cellular levels of calcein were normalized to protein determined by a micro bicinchoninic acid (BCA) protein assay kit (ThermoFisher). To test active vs passive transport, the calcein AM assay was run at 4°C.

Prior to transport experiments, cells were washed with phenol red free MEM. The following substrates were added to the basolateral chamber to measure P-gp or BCRP transport: 5 μM rhodamine 123 (R123) (Invitrogen), 10 μg/mL doxorubicin (LC Laboratories) or 5 μM BODIPY-FL-prazosin (Invitrogen). The microdevices, 15 μM CSA (Sigma-Aldrich), or 50 μM Ko143 (Sigma-Aldrich) were added to the apical chamber and incubated at 37°C. CSA and Ko 143 are small molecule positive control inhibitors for P-gp and BCRP, respectively. The apical chamber was sampled over time and the fluorescence was measured using excitation (nm)/emission (nm) 495/560 (R123), 490/590 (doxorubicin), or 485/530 (prazosin). To account for passively absorbed drug in the microdevices, the microdevices were removed after the experiment and placed in an eppendorf tube. The microdevices are centrifuged at 500 g for 4 minutes and the supernatant is removed, sampled, and the fluorescence is measured. Fresh buffer is added to wash the microdevices. This process is

repeated until there is no detectable fluorescence in the supernatant. The amount of drug absorbed into the microdevices was accounted for in calculating the amount of drug transported. Transport function recovery was studied after microdevice removal. The control, positive control, and microdevice wells were washed and phenol red free MEM was added to the apical chamber. The fluorescence in the apical chamber was sampled and measured over time. The apparent permeability coefficient was calculated according to the equation:

$$P_{app} = \left(\frac{dQ}{dt}\right) * \left(\frac{1}{AC_o}\right)$$

where P_{app} is the apparent permeability (cm/s), dQ/dt (μg/s) is rate of drug transport, A is surface area of the transwell, and C_0 (μg/mL) is the initial drug concentration. Transwells without microdevices were used as controls. Transepithelial electrical resistance (TEER) is measured at each time point. Apical to basal transport is studied by adding the drug substrate at the concentrations indicated above to the apical chamber with the microdevices or positive control inhibitors. The basal chamber is then sampled and analyzed.

Biosimilar Mucus Transport Study

Biosimilar mucus consisting of 5% (w/v) mucin, 0.11% (w/v) linoleic acid, 0.36% (w/v) cholesterol, 0.18% (w/v) phosphatidylcholine, 0.163% (w/v) polysorbate 80, and 3.1% (w/v) BSA was prepared based on previously described methods.[34] Biosimilar mucus at 250 μL/cm^2, which is approximately 2 mm in thickness, was placed on the cultured Caco-2 cells in transwells. The mucus was incubated for 1 hour prior to the addition of microdevices, phenol red free MEM (control), or CSA in the apical chamber and 5 μM R123 in the basolateral chamber. Transport assays were performed as described above. After the experiment was complete, the mucus layer was removed and the microdevices were visualized on the Caco-2 cells by microscopy.

Passive Permeability

The passive transport of 4kDa FITC Dextran (Sigma-Aldrich) across the Caco-2 cell monolayer was performed as previously shown.[35] Briefly, Caco-2 cells well grown on transwells for 21 days. FITC Dextran (2 mM, 4kDa) was added to the apical chamber with and without microdevices. The basal chamber was sampled, and the fluorescence was measured over time (Ex 485 nm/Em 530 nm). All experiments were done in triplicate at 37°C.

Flow Cytometry of Cell Surface P-gp

The cell surface P-gp was labeled with fluorescent anti-P-gp monoclonal antibody (BD, Clone 17F9) and analyzed by flow cytometry. Briefly, Caco-2 cells grown on transwells for 21 days were washed with phenol red free MEM. Microdevices were added to the apical chamber for 3 hours at 37°C. After 3 hours, the cells were removed from the transwell membrane with cell dissociation buffer. The cells were washed 3X and then incubated with Alexa Fluor 488-conjugated mouse anti-P-gp monoclonal antibody at 4°C for 30 min. The cells were then washed 3X with 2% BSA and analyzed by flow cytometry. Two transwells

were combined for each sample to increase the cell number for flow cytometry. Transwells without microdevices were used as controls.

mRNA Expression of Efflux Transporters

Microdevices were added to transwells cultured with Caco-2 cells for 21 days. After 3 hours, RNA was collected from the transwell using RNeasy Mini kit (Qiagen). cDNA was generated from RNA with iScript cDNA Synthesis Kit (Bio-Rad). qPCR reactions were performed with SYBR Green PCR Master Mix (Applied Biosystems). L19 is used as a reference control. Samples are compared to transwells without microdevices as a treatment control.

Ex-vivo Mouse Model

Three BALB/c mice were sacrificed at 18–20 weeks of age. Jejenum of the intestine was isolated and solid waste was removed. The jejenum was sectioned into 4 cm long pieces. One end of the intestine was closed with a suture and 5 μM R123 was pipetted into the intestine section containing microdevices, CSA, or a control without treatment on the mucosal side. The other end of the intestine was tied off before the start of the experiment. The intestinal sacs were incubated in a 24 well plate in media at 37°C. The solution on the serosal side was removed, replaced with fresh media, and the fluorescence was measured at excitation 495 nm /emission 560 nm over time. After the final sample was taken, the intestine was removed and measured to determine the surface area.

Mouse Studies

All mouse experiments were approved by the institutional animal care and use committee (IACUC) at Carnegie Mellon University (Pittsburgh, PA, USA) under protocol number PROTO201600017, and were performed in accordance with all institutional, local, and federal regulations. C57BL/6 mice were either purchased from Charles River Laboratories (Wilmington, MA, USA) or obtained from an institutionally managed breeding colony. Prior to experiments, mice were housed in cages of no more than five animals, with controlled temperature (25°C), 12 hour light-dark cycles, and free access to food and water. Mice utilized in this study were male and 8 – 16 weeks old (16 – 26 grams). The free-to-use PS power calculator (Vanderbilt) was used to determine the minimal sample size for which statistical power was greater than or equal to 0.8. (n = 5 – 7). Mice were fasted for 12 hours the night before an experiment to limit the variability caused by food matter and feces in the GI tract. Oral gavages and phosphate buffered saline (PBS) rehydration were administered at a volume of 10 ml solution per kg of mouse body weight (10 μL/g).

Oral Delivery of Rhodamine 123

Fasted mice were orally gavaged with one of three treatment solutions: 40,000 microdevices/mL solution (400,000 microdevices/kg total dose), 0.5 mg/mL (5 mg/kg) cyclosporine A (CSA) as a positive control, or phosphate buffer saline (PBS) as a negative control. Every treatment also contained 9.6 mg/mL (96 mg/kg) BSA to stabilize the solution. Thirty minutes (controls) or two hours (microdevices) later, submandibular blood was collected from each mouse to provide baseline fluorescent values, and each mouse received

a gavage of 0.4 mg/mL (4 mg/kg) R123. Submandibular blood was collected at 10, 20, 30, and 60 minutes following the R123 gavage, and mice received subcutaneous PBS rehydration after the 30 and 60 minute blood draws. At 240 minutes, the mice were euthanized and final blood collected via cardiac puncture.

All samples were centrifuged to isolate the serum, which was removed and examined for R123 concentration by reading for fluorescence on a Tecan Spark® automated plate reader (495/560 nm). Application of a R123 calibration curve, in the presence of mouse serum, yielded the reported concentrations of the model drug in each sample.

Statistics

Statistical analysis was performed by a two-way ANOVA with a Tukey's multiple comparison correction to determine significance between groups. Analysis between two groups was performed by a two-tailed t-test. Plots show mean ± standard deviation (SD) where * represents $p<0.05$, ** represents $p<0.01$, and *** represents $p<0.001$.

Results and Discussion

Microdevice Characterization

Uniform 200 μm biocompatible PEG microdevices were fabricated by photolithography. Briefly, PEGDMA, deionized water, and initiator (IRGACURE) were mixed and a thin layer was added to a silicon wafer. The mixture was irradiated through a 200 μm mask to form crosslinked microdevices (Figure 1A). Microdevices were visualized with bright field microscopy (20 μm × 200 μm) (Figure 1B). Microdevices did not alter cell viability or metabolic activity as indicated by staining of dead cells with propidium iodide (PI) and with a Presto Blue assay which measured the reducing power of living cells (Figure 2A). The microdevices also did not affect ATP amounts, indicating viable cells (Figure 2A).

In Figure 2B, microdevices were visualized on top of cells with confocal microscopy. Microdevices were added for 3 hours on a Caco-2 monolayer grown on transwells for 21 days. Immunostaining shows an intact confluent monolayer of Caco-2 cells expressing actin underneath the devices (Figure 2B).

Microdevice inhibition of efflux transporters

Efflux transporters decrease oral bioavailability by pumping drugs that get absorbed into the intestinal cells back out into the GI lumen, preventing drugs from entering the systemic circulation.[6] First, the effects of the microdevices on P-gp function were tested. P-gp is a critical efflux transporter in the intestine with a broad substrate specificity and a determinant of oral bioavailability of many drug substrates from chemotherapeutics to immunosuppressants.[7] Microdevices were shown to inhibit the transport of multiple model P-gp substrates, including calcein AM, doxorubicin, and R123. Calcein AM, a non-fluorescent P-gp substrate that freely diffuses into the cell is rapidly cleaved intracellularly by esterases to form fluorescent calcein, which is not a P-gp substrate. Inhibition of P-gp results in an accumulation of calcein AM inside the cell and a corresponding increase in hydrolysis to calcein and higher fluorescence. Microdevices (3000 microdevices/cm^2)

increased the intracellular concentration of calcein to a similar degree as a positive control small molecule inhibitor, CSA, indicating P-gp inhibition (Figure 3A). P-gp inhibition by microdevices was also studied in a transwell system where the Caco-2 cells were cultured on transwell membrane inserts for 21 days (Figure 1C). The TEER at the time of study was greater than 350 Ω•cm^2, indicating tight epithelial junctions. Doxorubicin is a chemotherapeutic which freely diffuses into the cell when added to the basal chamber and then gets transported by P-gp into the apical chamber. Microdevices at 3000 microdevices/cm^2 were placed on the Caco-2 cells in a transwell decreased efflux of doxorubicin into the apical chamber, consistent with P-gp inhibition (Figure 3B). The apparent permeability (P_{app}) is defined by the drug transport rate, initial drug concentration, and the surface area of the transwell insert. P_{app} decreased in Caco-2 cells with the microdevices or when treated with CSA (Table 2). The P-gp substrate R123 was also tested in Caco-2 transwells. R123 was added to the basolateral chamber and transported into the cell where it is subsequently effluxed into the apical chamber by P-gp. We tested whether the level of inhibition was dependent on the dose of microdevices with the addition of 3000 microdevices/cm^2 or 900 microdevices/cm^2 to the apical chamber. While we have seen significant decrease of R123 with both doses compared to control, the 3000 microdevices/cm^2 showed a higher degree of inhibition more similar to CSA (Figure 3C). The P_{app} decreased with the microdevices and CSA (Table 2). To test whether the microdevices permanently alter transporter function, we performed a transporter recovery assay. R123 transport by P-gp recovered following removal of the microdevices to levels comparable to cells without microdevices, indicating reversible inhibition of P-gp (Figure 3D). Reversibility of transporter function is important as these efflux transporters function to prevent toxic material from entering systemic circulation. Therefore, permanently decreasing transporter function could result in toxic adverse effects.[7,8]

Since there is significant overlap between P-gp and BCRP substrates, the effects of the microdevices on BCRP function were also tested using the BCRP substrate BODIPY-FL-prazosin (prazosin). Prazosin freely diffuses into the cell and is effluxed out on the apical membrane by BCRP. As a positive control we used a potent BCRP specific inhibitor, Ko143. Microdevices (3000 microdevices/cm^2) decreased basal to apical transport (Figure 4) and decreased the prazosin P_{app} to a similar degree as Ko143 (Table 2). As shown previously, efflux transporters often work in concert with each other, with one efflux transporter increasing function in response to loss of function of another efflux transporter, thus limiting drug absorption.[36] Inhibition of both P-gp and BCRP by the hydrogel microdevices is predicted to enhance the increase in intestinal absorption.

The P-gp and BCRP substrates used in these studies diffuse into the cells when placed on the basolateral side of Caco-2 cells. P-gp then actively transports R123 and doxorubicin while BCRP transports prazosin out of the cell into the apical compartment. Measurement from the basal to apical chamber allows for direct measurement of the function of the efflux transporters. Others have shown that there is minimal to no difference in the absence and presence of an inhibitor when these substrates are added to the apical side and detected on the basolateral side.[37–41] We see similar results with established P-gp and BCRP inhibitors, likely due to an insufficient change in the concentration gradient in the presence of inhibitor to detect concentration differences in the basolateral chamber (Supporting Information 3).

Microdevices function through biosimilar mucus

The intestine has multiple barriers to prevent drug absorption, including the intestinal mucus. Although the mucus acts as a protective barrier to prevent bacterial microbes and toxic material from reaching the epithelial cells, it can also prevent drugs and drug delivery formulations from interacting with these cells. A biosimilar mucus was used to test the effects of the microdevices in a transwell system.[34] The mucus was added to the apical chamber and allowed to incubate for 1 hour. Afterwards, the P-gp substrate R123 was added to the basal chamber and 3000 microdevices/cm^2 were added on top of the mucus layer. Similar to the experiments without mucus, microdevices inhibited P-gp as indicated by a decrease in R123 flux into the apical chamber; however, this inhibition of P-gp was delayed due to the need for the devices to permeate through the mucus for access to the transporter (Figure 5). While the effect of the microdevices on P-gp occurred within 2 hours without the mucus layer, inhibition was not detected until 4 hours after adding the microdevices with the mucus. Interestingly, the inhibitory effect of the microdevices was greater than that of CSA in the presence of mucus. This may be due to the small molecule being entrapped in the mucus and unable to interact with P-gp on the cell membrane. The microdevices were visible on the Caco-2 monolayer upon removal of the mucus layer. We hypothesis due to the weight and size of the microdevices that they are able to displace the mucus layer allowing them to travel through the mucus to interact with the membrane transporters on the cell surface. Compared to control, P_{app} decreases with microdevices to a similar extent as with CSA (Table 2). As the mucosal layer is a barrier to cell accessibility and drug absorption, the ability of the microdevices to penetrate this mucosal layer is critical for interaction with the intestinal cells to inhibit efflux transport.

Microdevices affect P-gp function by decreasing cell surface expression

The possibility that the microdevices inhibit drug permeation by altering tight junctions was evaluated by measuring permeation of 4kDa FITC dextran. In the Caco-2 transwell system, the P_{app} for the 4kDa FITC dextran solution and the percentage that permeates the cell monolayer was unchanged with the addition of 3000 microdevices/cm^2 (4.7% permeation after 4 hours in the absence and presence of microdevices), indicating that the microdevices are not affecting paracellular drug transport (Figure 6A). To further test if the transport mechanism is active or passive, transport studies were performed at 4°C and 37°C. Inhibition of calcein AM transport with the microdevices was only apparent when the cells were kept at 37°C, indicating active transport is required for microdevice function (Figure 6B). In addition, we do not observe any changes in TEER with the microdevices present indicating the microdevices are not affecting paracellular drug permeation (Supporting Information 2).

The effect of the microdevices on P-gp expression was also considered. To test whether the microdevices were affecting transporter expression levels on the mRNA level, qPCR was performed. P-gp and BCRP mRNA levels remain unaltered after 3 hours of treatment with the microdevices compared to control (Figure 7A). Due to the short time scale of hours in the microdevice treatment, a change in mRNA levels is not necessarily expected. To further test if a direct change in cell surface P-gp protein amounts were altered in the presence of the microdevices we performed flow cytometry. Briefly, Caco-2 cells grown on transwells

were exposed to microdevices for 3 hours, stained with a P-gp antibody that recognizes an external epitope, and analyzed by flow cytometry. Exposure to the microdevices caused a decrease in levels of P-gp on the cell membrane when compared to untreated cells (Figure 7B). We propose that the decrease in cell surface P-gp is due to the interactions with the microdevices, which then leads to decreased P-gp function. The structure of P-gp in the transmembrane domain has been shown to be tightly integrated with cholesterol and phospholipids, and this interaction is critical for transporter dynamics.[42] Whether the microdevices affect P-gp function by disrupting these interactions requires investigation. Consistent with previous work, altering the cell surface interactions of the transporter can indeed affect transporter function.[43] Additionally, it is plausible that the microdevices sterically hinder the conformational changes required for P-gp to release a substrate from the binding site in the transmembrane region to the apical chamber, resulting in P-gp inhibition. Such steric hinderance could also lead to internalization of the transporter as supported by the decrease membrane expression after exposure to microdevices (Figure 7B).

Ex Vivo mouse model to measure R123 transport

Ex vivo models allow for increased complexity of intestinal epithelium interactions over 2D culture methods while allowing for higher throughput over *in vivo* studies.[44] We isolated and sectioned the mouse jejunum into 4 cm regions to generate intestinal sacs. The intestinal sacs were loaded with R123 in the absence or presence of 3000 microdevices/cm^2 or CSA on the mucosal side. The intestine was closed on both sides and transport of R123 across the intestinal barrier of the epithelial cells was measured on the serosal side. We showed a significant increase in transport of R123 to the serosal side in the presence of microdevices compared to control (Figure 8). The P_{app} increases in the presence of microdevices compared to control. This suggests that the microdevices were able to inhibit P-gp in a physiological *ex vivo* model, increasing drug transport across the cell to the serosal side. This *ex vivo* model better represents an *in vivo* oral dose where the drug substrate is interacting with the epithelial cells on the mucosal side to increase drug absorption to the serosal side.

In vivo mouse model to measure R123 Transport

In vivo mouse models represent a more physiological environment where mucus, microbiome, and peristalsis flow which are difficult to represent *in vitro* are intact. Microdevices (400,000 microdevices/kg total dose), or CSA were given by gavage to C57BL/6 mice after a 12-hour fasting period. Microdevices were preincubated for 2 hours while CSA was preincubated for 30 minutes, then R123 was given by oral gavage to the mice. Blood was collected over time through a submandibular vein. A significant increase in R123 C_{max} was measured with CSA and microdevices compared to control (Figure 9). The C_{max} and $AUC_{0–60min}$ increase is consistent with changes in the absorption phase of R123. Previous studies in rodents demonstrated rapid systemic hydrolysis of R123 to the corresponding acid, R110.[45,46] Since the fluorescence assay used to detect R123 will also detect R110, it is difficult to interpret potential effects on the elimination phase of R123, although inhibition of P-gp in the liver or kidney is not expected since the microdevices are too large to be absorbed. This suggests that microdevices are able to inhibit P-gp *in vivo*,

even with multiple barriers in the stomach and intestine, leading to increased R123 absorbed into systemic circulation.

Conclusions

The importance of gut efflux transporters in limiting drug absorption is well recognized. Attempts at inhibiting efflux transporters as a strategy to improve bioavailability have been limited by adverse events.[15] Thus, there is a critical need for novel strategies to inhibit efflux transporters to improve oral drug absorption, particularly for drug substrates such as chemotherapeutics and immunosuppressants. Here, a materials-based approach was applied to study the effects of biocompatible crosslinked PEGDMA materials and their effects on efflux transporters. Due to the frequent use of PEG based materials in oral drug delivery, it is important to better understand the cellular-level effects of these materials as they interact with the intestinal epithelium. Here we demonstrated that PEGDMA microdevices inhibit P-gp and BCRP in a transwell Caco-2 model. The inhibition of P-gp was dose dependent with a greater number of microdevices resulting in increased P-gp inhibition. Dose dependence allows for control of the degree of inhibition based on drug or patient characteristics. In addition, the P-gp inhibition was completely reversible upon the removal of the microdevices. Importantly, the microdevices can function as P-gp inhibitors through a biosimilar mucus *in vitro* and increase mucosal to serosal drug transport in an *ex vivo* mouse intestinal sac model. Furthermore, in an *in vivo* mouse model, the microdevices increase C_{max} and $AUC_{0–60min}$ of R123 compared to control, indicating the microdevices are acting as P-gp inhibitors *in vivo*. The decrease in P-gp function is likely due at least in part to a reduction in P-gp on the cell membrane in the presence of the microdevices.

Since the microdevices only interact with the surface of the intestinal cell and do not enter systemic circulation, our approach presents a nonpharmacological method to inhibit P-gp with the goal to limit toxicity and adverse effects from current small molecule inhibitors. These findings open new possibilities for oral P-gp inhibition with the potential to locally and reversibly inhibit P-gp using microdevices. A more extensive characterization of the mechanism by which microdevices inhibit P-gp is required to fully understand their interaction with gut P-gp and to support novel therapeutic approaches to improve oral drug bioavailability. While a representative fluorescent P-gp substrate, R123, was used as a model substrate, this system can be translated to drugs that have limited oral bioavailability due to P-gp efflux. Moreover, the knowledge gained in this study will be broadly useful in the design of hydrogel-based oral delivery systems, particularly with drugs that are efflux transporter substrates.

Supplementary Material

Refer to Web version on PubMed Central for supplementary material.

Acknowledgments

This work was supported by NIH R01EB018842 to T.A.D. E.S.L. was supported by the American Foundation for Pharmaceutical Education, Advancing Science in American Fellowship Foundation, and by the NIH Training Grant 5T32GM007175-27. K.E.S. was supported by NSF Graduate Fellowship DGE-1106400 and N.G.L. was supported by NSF Graduate Fellowship DGE-1252522. Confocal fluorescence imaging was conducted at the UCSF Nikon

Imaging Center. The authors would like to thank Serena Tamura for providing mouse tissue for the *ex vivo* experiments.

References

1. Sastry S, Nyshadham J & Fix J Recent technological advances in oral drug delivery - a review. Pharm. Sci. Technolo. Today 3, 138–145 (2000). [PubMed: 10754543]
2. Gupta H, Bhandari D & Sharma A Recent trends in oral drug delivery: a review. Recent Pat. Drug Deliv. Formul 3, 162–173 (2009). [PubMed: 19519576]
3. Verma RK, Mishra B & Garg S Drug Development and Industrial Pharmacy Osmotically Controlled Oral Drug Delivery. Drug Dev. Ind. Pharm 267, 695–708 (2000).
4. Ensign LM, Cone R & Hanes J Oral drug delivery with polymeric nanoparticles: The gastrointestinal mucus barriers. Adv. Drug Deliv. Rev 64, 557–570 (2012). [PubMed: 22212900]
5. Goldberg M & Gomez-Orellana I Challenges for the oral delivery of macromolecules. Nat. Rev. Drug Discov 2, 289–95 (2003). [PubMed: 12669028]
6. Chan LMS, Lowes S & Hirst BH The ABCs of drug transport in intestine and liver: efflux proteins limiting drug absorption and bioavailability. Eur. J. Pharm. Sci 21, 25–51 (2004). [PubMed: 14706810]
7. Amin ML P-glycoprotein Inhibition for Optimal Drug Delivery. Drug Target Insights 7, 27–34 (2013). [PubMed: 24023511]
8. Lin JH & Yamazaki M Role of P-Glycoprotein in Pharmacokinetics. Clin. Pharmacokinet 42, 59–98 (2003). [PubMed: 12489979]
9. Lomovskaya O & Bostian KA Practical applications and feasibility of efflux pump inhibitors in the clinic—A vision for applied use. Biochem Pharmacol. 71:7, 910–8 (2006) [PubMed: 16427026]
10. Giacomini KM et al. Membrane transporters in drug development. Nat. Rev. Drug Discov. 9, 215–236 (2010). [PubMed: 20190787]
11. International Transporter Consortium TIT et al. Membrane transporters in drug development. Nat. Rev. Drug Discov. 9, 215–36 (2010). [PubMed: 20190787]
12. Karolewicz B A review of polymers as multifunctional excipients in drug dosage form technology. Saudi Pharm. J 24, 525–536 (2016). [PubMed: 27752224]
13. Varma MVS, Ashokraj Y, Dey CS & Panchagnula R P-glycoprotein inhibitors and their screening: a perspective from bioavailability enhancement. 48, 347–359 (2003).
14. Robert J, Jarry C Multidrug Resistance Reversal Agents. J. Med. Chem 46:23, 4805–4817 (2003). [PubMed: 14584929]
15. Raghava KM & Lakshmi PK Overview of P-glycoprotein inhibitors: A rational outlook. Brazilian J. Pharm. Sci 48, 353–367 (2012).
16. Robey, R. W., Massey, P. R, Amiri-Kordestani L & Bates, S. E ABC Transporters: Unvalidated Therapeutic Targets in Cancer and the CNS. Anticancer. Agents Med. Chem 10, 625–633 (2011).
17. Tamaki A, Ierano C, Szakacs G, Robey RW & Bates SE The controversial role of ABC transporters in clinical oncology. Essays Biochem. 50, 209–232 (2011). [PubMed: 21967059]
18. Yuan Y et al. Nanoparticle delivery of anticancer drugs overcomes multidrug resistance in breast cancer. Drug Deliv. 23, 3350–3357 (2016). [PubMed: 27098896]
19. Kam KR et al. Nanostructure-mediated transport of biologics across epithelial tissue: Enhancing permeability via nanotopography. Nano Lett. 13, 164–171 (2013). [PubMed: 23186530]
20. Fox CB et al. Fabrication of Sealed Nanostraw Microdevices for Oral Drug Delivery. doi:10.1021/acsnano.6b00809
21. Gupta P, Vermani K & Garg S Hydrogels: From controlled release to pH-responsive drug delivery. Drug Discovery Today (2002). doi:10.1016/S1359-6446(02)02255-9
22. Sharpe LA, Daily AM, Horava SD & Peppas NA Therapeutic applications of hydrogels in oral drug delivery. Expert Opin. Drug Deliv. 11, 901–15 (2014). [PubMed: 24848309]
23. Puranik AS, Pao LP, White VM & Peppas NA In Vitro Evaluation of pH-Responsive Nanoscale Hydrogels for the Oral Delivery of Hydrophobic Therapeutics. Ind. Eng. Chem. Res 55, 10576–10590 (2016).

24. Horava SD, Moy KJ & Peppas NA Biodegradable hydrophilic carriers for the oral delivery of hematological factor IX for hemophilia B treatment. Int. J. Pharm 514, 220–228 (2016). [PubMed: 27863665]
25. Culver HR et al. HHS Public Access. 50, 170–178 (2018).
26. Dash AK & Ii GCC Therapeutic Applications of Implantable Drug Delivery Systems. 12, 1–12 (1999).
27. Larrañeta E, Stewart S, Ervine M, Al-Kasasbeh R & Donnelly RF Hydrogels for hydrophobic drug delivery. Classification, synthesis and applications. J. Funct. Biomater 9, (2018).
28. Lin CC & Anseth KS PEG hydrogels for the controlled release of biomolecules in regenerative medicine. Pharm. Res 26, 631–643 (2009). [PubMed: 19089601]
29. Hugger ED, Audus KL & Borchardt RT Effects of poly(ethylene glycol) on efflux transporter activity in Caco-2 cell monolayers. J. Pharm. Sci 91, 1980–1990 (2002). [PubMed: 12210045]
30. Hodaei D, Baradaran B, Valizadeh H & Zakeri-milani P Effects of polyethylene glycols on intestinal efflux pump expression and activity in Caco-2 cells. Braz. J. Pharm. Sci 51, (2015).
31. Shen Q et al. Modulation of intestinal P-glycoprotein function by polyethylene glycols and their derivatives by in vitro transport and in situ absorption studies. Int. J. Pharm 313, 49–56 (2006). [PubMed: 16500056]
32. Chirra HD et al. Planar Microdevices for Enhanced In Vivo Retention and Oral Bioavailability of Poorly Permeable Drugs. Adv. Healthc. Mater 3, 1648–1654 (2014). [PubMed: 24711341]
33. Le LV et al. Injectable hyaluronic acid based microrods provide local micromechanical and biochemical cues to attenuate cardiac fibrosis after myocardial infarction. Biomaterials 169, 11–21 (2018). [PubMed: 29631164]
34. Boegh M, Baldursdóttir SG, Müllertz A & Nielsen HM Property profiling of biosimilar mucus in a novel mucus-containing in vitro model for assessment of intestinal drug absorption. Eur. J. Pharm. Biopharm 87, 227–235 (2014). [PubMed: 24413146]
35. Kowapradit J et al. In vitro Permeability Enhancement in Intestinal Epithelial Cells (Caco-2) Monolayer of Water Soluble Quaternary Ammonium Chitosan Derivatives. AAPS PharmSciTech 11, 497–508 (2010). [PubMed: 20333490]
36. DeVries NA et al. P-glycoprotein and breast cancer resistance protein: Two dominant transporters working together in limiting the brain penetration of topotecan. Clin. Cancer Res. 13, 6440–6449 (2007). [PubMed: 17975156]
37. Stormer E, et al. Methadone Inhibits Rhodamine123 Transport in Caco-2 Cells. Drug Metab. Dispos 30, 483–487 (2002). [PubMed: 11950775]
38. Chimezie C et al. Glyceollin Transport, Metabolism, and Effects on P-Glycoprotein Function in Caco-2 Cells. J. Med. Food 17, 462–471 (2014). [PubMed: 24476214]
39. Sugihara N et al. Effect of benzo [a] pyrene on P-glycoprotein-mediated transport in Caco-2 cell monolayer. Toxicology. 223, 156–165 (2006). [PubMed: 16647797]
40. Li Y et al. Phorbol 12-myristate 13-acetate inhibits P-glycoprotein-mediated efflux of digoxin in MDCKII- MDR1 and Caco-2 cell monolayer models. Nat. Publ. Gr 35, 283–291 (2013).
41. Oga EF, Sekine S, Shitara Y & Horie T Potential P-Glycoprotein-Mediated Drug-Drug Interactions of Antimalarial Agents in Caco-2 cells. Am. J. Trop. Med. Hyg 87, 64–69 (2012). [PubMed: 22764293]
42. Alam A, Kowal J, Broude E, Roninson I & Locher KP Structural insight into substrate and inhibitor discrimination by human P-glycoprotein. Science. 363, 753–756 (2019). [PubMed: 30765569]
43. Dai Z, Yao Q & Zhu L MMP2-Sensitive PEG-Lipid Copolymers: A New Type of Tumor-Targeted P-Glycoprotein Inhibitor. ACS Appl. Mater. Interfaces 8, 12661–12673 (2016). [PubMed: 27145021]
44. Goggin BJ et al. Intestinal Sacs to Assess Mucosal Permeability in Models of Gastrointestinal Disease. J. Vis. Exp 199, 1–7 (2016).
45. Zhao W et al. Effects of Polyoxyethylene Alkyl Ethers on the Intestinal Transport and Absorption of Rhodamine 123: A P-glycoprotein Substrate by in Vitro and in Vivo Studies. J. Pharm. Sci 105, 1526–1534 (2016). [PubMed: 26968974]

46. Forster S, Thumser AE, Hood SR & Plant N Characterization of rhodamine-123 as a tracer dye for use in in vitro drug transport assays. PLoS One 7, (2012).

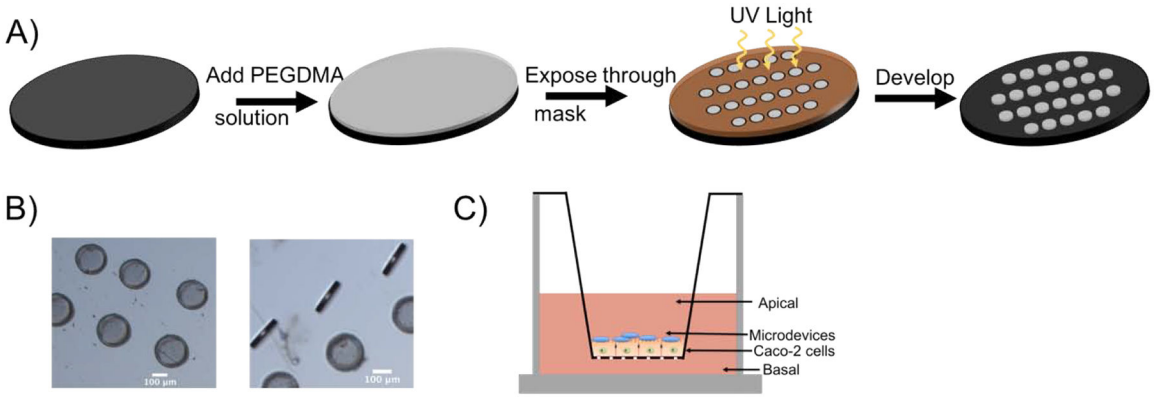

Figure 1.

Fabrication of 20 μm × 200 μm PEGDMA microdevices using photolithography. A) Schematic representation of the microdevice formation using ultraviolet (UV) light irradiation. B) Brightfield (5X) image of microdevices. Scale bar 100 μm. C) Transwell model system with Caco-2 cells grown on transwell insert membrane for 21 days and microdevices added to the apical surface of the intestinal monolayer.

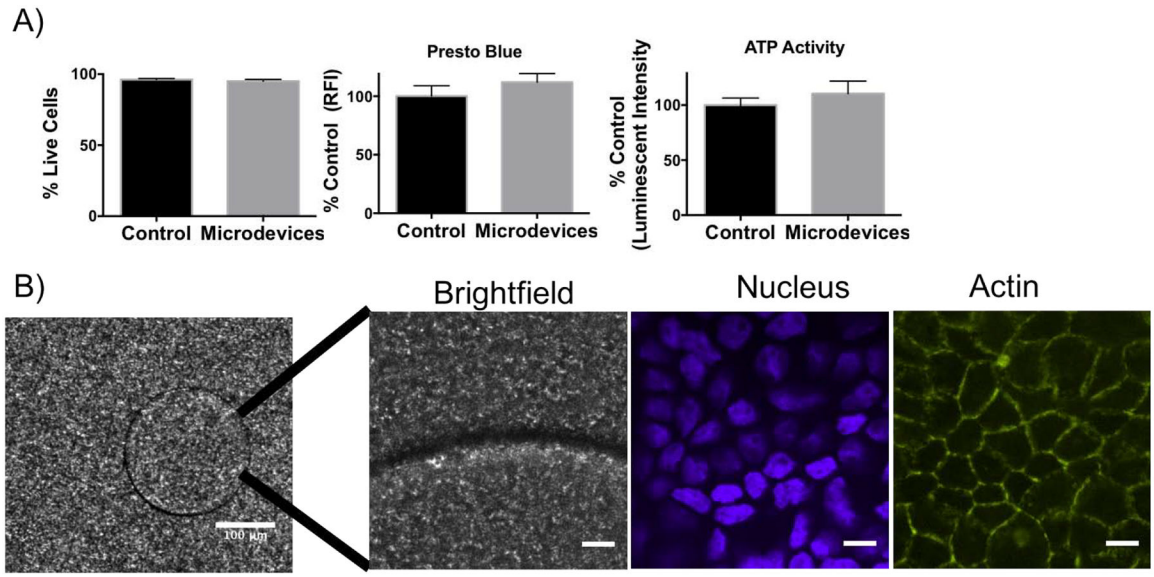

Figure 2.

Characterization of microdevices in Caco-2 cells. A) Biocompatibility studies of the microdevices on Caco-2 cells with a propidium iodide (dead) stain, PrestoBlue assay, and ATP assay (two-tailed t-test, Mean ± SD; n=3). B) Fluorescence confocal images (10X) of microdevice (Scale Bar =100 μm) and of microdevices incubated for 3 hours on Caco-2 cells grown on transwells for 3 weeks (60X) showing the microdevices in brightfield (BF), DAPI nucleus (blue) stain, and phalloidin actin (green) (representative image of n=3 wells). Scale Bar =10 μm.

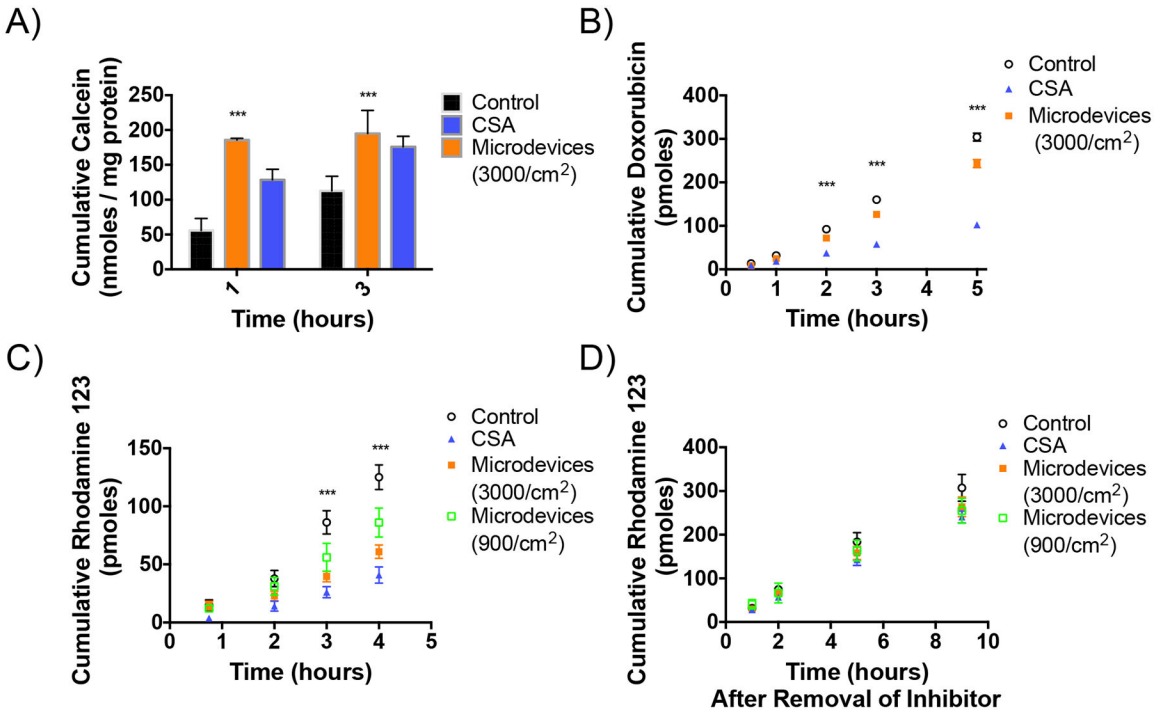

Figure 3.

Inhibition of P-gp transport by microdevices in Caco-2 cells. A) Caco-2 cells were grown on 96 well plates for 14 days before measurement of intracellular calcein AM transport. Both the canonical P-gp inhibitor CSA and microdevices (3000 microdevices/cm^2) inhibited P-gp as indicated by increased intracellular calcein concentrations (two-way ANOVA, Mean ± SD; ***p<0.0001; n=3). B) Caco-2 cells were grown on transwell membranes for 21 days prior to measurement of doxorubicin flux from the basolateral to apical compartments. The values shown are the cumulative amounts of doxorubicin transported into the apical chamber at each time (two-way ANOVA, Mean ± SD; ***p<0.0001; n=3). Doxorubicin flux was decreased by microdevices (3000 microdevices/cm^2) and CSA. Shown is one representative experiment of 3 independent experiments (Supporting Information 5). C) R123 flux from the basal to apical chamber was measured in the presence and absence of microdevices and CSA. The values shown are the cumulative amounts of R123 measured in the apical chamber (two-way ANOVA, Mean ± SD; ***p<0.0001 w.r.t. untreated control; n=3). Microdevices and CSA both inhibited R123 flux and more inhibition of P-gp was seen with 3000 devices/cm^2 than 900 devices/cm^2. The two microdevice doses are significantly different at T=3 (* p<0.05) and T=4 (*** p<0.0001). Shown is one representative experiment of 4 independent experiments (Supporting Information 4). D) Recovery experiment with R123 where devices are removed, and transport into the apical chamber is measured over time. No difference is seen between the conditions once the devices are removed (two-way ANOVA, Mean ± SD; n=3).

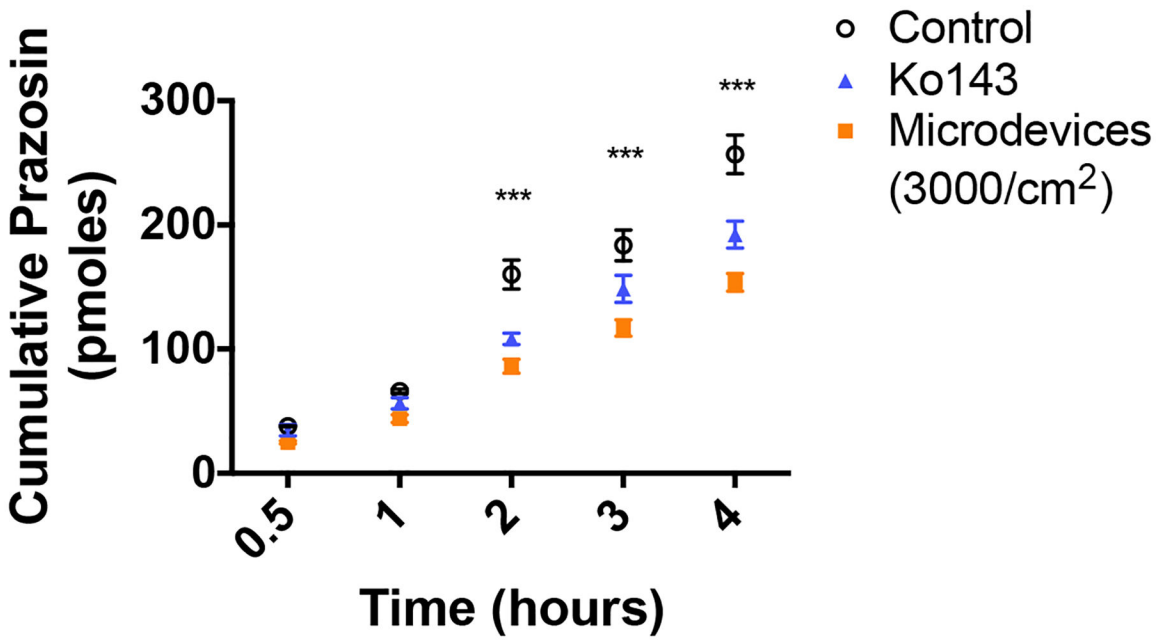

Figure 4.

Microdevices (3000 microdevices/cm^2) inhibit BCRP transport in Caco-2 cells. Caco-2 cells were grown on transwell membranes for 21 days prior to measurement of prazosin transport. The values shown are the cumulative amounts of prazosin measured in the apical chamber (two-way ANOVA, Mean ± SD; ***p<0.0001 w.r.t. untreated control; n=3). Microdevices inhibit prazosin transport to a similar degree as CSA. Shown is one representative experiment of 3 independent experiments (Supporting Information 6).

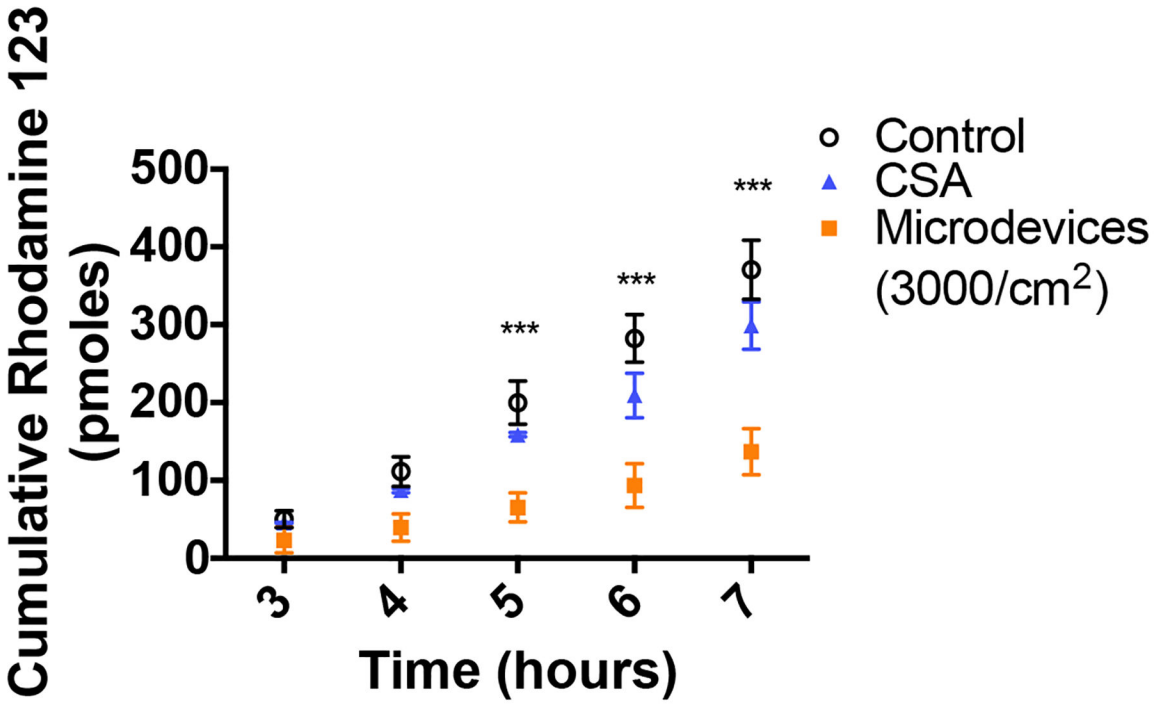

Figure 5.

Microdevices inhibit P-gp transport through biosimilar mucus. Caco-2 cells were grown on transwell membranes for 21 days prior to measurement of R123 flux from the basal to apical chamber in the presence and absence of microdevices (3000 microdevices/cm^2) and CSA. The values shown are the cumulative amounts of R123 measured in the apical chamber at specific times (two-way ANOVA, Mean ± SD; ***$p<0.0001$ w.r.t. untreated control; n=3). Microdevices and CSA both inhibited R123 flux under conditions of a biosimilar mucus layer. Shown is one representative experiment of 3 independent experiments (Supporting Information 7).

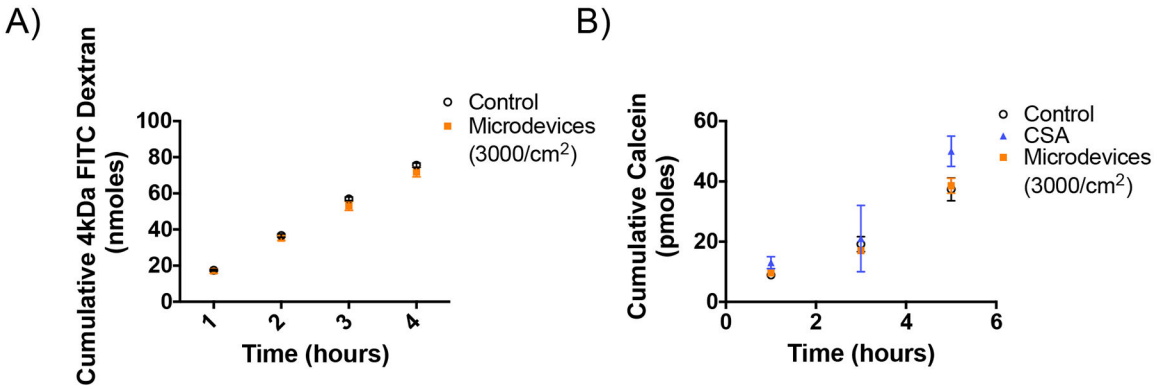

Figure 6.

Microdevices do not affect passive permeability of Caco-2 cells. A) Caco-2 cells were grown on transwells for 21 days prior to measurement of apical to basal flux of 4 kDa FITC Dextran transport. The values shown are means ±SD of 3 biological replications. There was no effect of the microdevices on FITC dextran flux indicating no effect on tight junctions. B) Caco-2 cells were grown on 96 well plates for 14 days prior to measurement of intracellular calcein concentrations at 4°C. The values shown are means ±SD of 3 biological replications. There was no effect of the microdevices on calcein accumulation at 4°C.

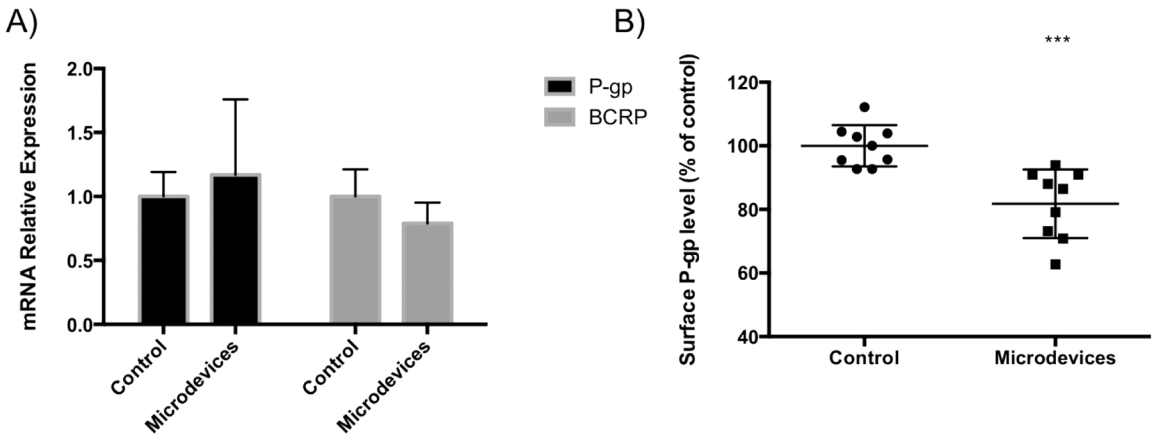

Figure 7.

Microdevices decrease cell surface P-gp levels in Caco-2 cells. Caco-2 cells were grown on transwells for 21 days and A) mRNA levels corresponding to P-gp (ABCB1) and BCRP (ABCG2) in the absence and presence of microdevice exposure for 3 hours were measured by qPCR. B) Following the same treatment of Caco-2 cells with microdevices, cell surface P-gp levels were analyzed by flow cytometry. P-gp levels are expressed relative to levels in cells without microdevices (two-tailed t-test, Mean ± SD; ***$p<0.0001$; n=9). Surface P-gp protein levels were decreased in cells after addition of the microdevices.

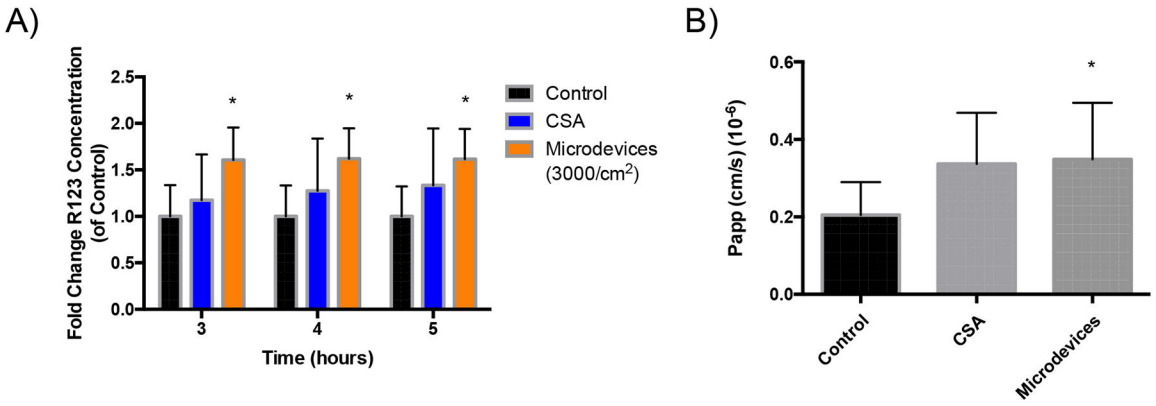

Figure 8.

Microdevices increase mucosal to serosal transport of R123 in an *ex vivo* mouse model. Jejunum was sectioned to form intestinal sacs where R123 transport was measured over time in the presence and absence of microdevices (3000 microdevices/cm^2) or CSA. A) Fold change of R123 transport compared to control, without microdevices. (Two-way ANOVA, Mean ± SD; *$p<0.05$ w.r.t. untreated control, n=6 Control, n=4 CSA, n=6 Microdevices) B) Calculated P_{app} of R123 transport with an increase in P_{app} from $0.2*10^{-6}$ cm/sec (control) to $0.35*10^{-6}$ cm/sec with microdevices and $0.33*10^{-6}$ cm/sec with CSA. R123 transport from mucosal to serosal side was increased with microdevices. (Two-tailed t-test, Mean ± SD;* $p<0.05$ w.r.t. untreated control, n=6 Control, n=4 CSA, n=6 Microdevices)

A)

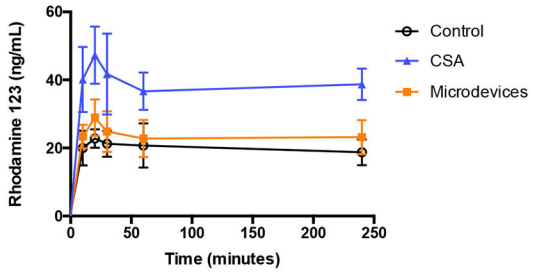

B)

	Control	CSA	Microdevices
C_{max} (ng ml^{-1})	22.78 ± 2.7	38.7 ± 4.6	28.92 ± 5.4
$AUC_{0\text{-}60min}$ (ng ml^{-1} h)	19.39 ± 3.5	37.5± 5.9	22.61 ± 4.2

Figure 9.

Microdevices increase systemic circulation of R123 in an *in vivo* mouse model. Oral gavage of microdevices (400,000 devices/kg), CSA, and R123 was performed on C57BL/6 mice where R123 transport was measured over time. A) Systemic R123 amounts measured in serum over time B) C_{max} and $AUC_{0–60min}$ values analyzed from the concentration-time curve (two-tailed t-test, Mean ± SD; C_{max} p=0.012 Control vs Microdevices; n=8 Control, n=5 CSA, n=8 Microdevices)

Table 1:

Gene and Primer Sequence for qPCR

Gene	Primer Sequence
MDR1	F 5'-GCC AAA GCC AAA ATA TCA GC 3' R 5'-TTC CAA TGT GTT CGG CAT 3'
ABCG2	F 5'-TGC AAC ATG TAC TGG CGA AGA 3' R 5'-TCT TCC ACA AGC CCC AGG 3'
L19	F 5'-TCGCCTCTAGTGTCCTCCG 3' R 5'- GCGGGCCAAGGTGTTTTTC 3'

Table 2.

P_{app} values of P-gp and BCRP substrates

P_{app} (cm/s) (10^{-6})	**Control**	**Inhibitor**	**Microdevices**
R123	8.03 ± 3.5	2.03 ± 0.71	5.51 ± 2.4
Doxorubicin	1.90 ± 0.35	1.33 ± 0.46	1.74 ± 0.25
Prazosin	10.18 ± 0.25	8.21 ± 0.90	7.36 ± 1.7
R123 with mucus	9.25 ± 3.8	3.53 ± 3.5	4.21 ± 0.51

P_{app} was calculated in 3–4 independent experiments and the mean ±SD are represented in the table.